Wave Drag Analysis of Realistic Fighter Aircraft Using a Full-Potential Method

Kenneth B. Walkley* and Gregory E. Smith†
Dynamic Engineering, Inc., Newport News, Virginia

Wave drag coefficients for several aircraft configurations have been computed using a full-potential method and have been compared with the results of parallel far-field (area rule) analyses and experimental zero-lift drag data. The aircraft analyzed included a supersonic cruise configuration, an advanced fighter concept, and the F-16 aircraft. The results of these studies indicate that the full-potential method generally gives wave drag levels that agree more closely with test data than do the far-field values. The full-potential method does not encounter problems when components such as wing or tail leading edges or canopy forward faces are at sonic conditions, as does the far-field technique. The full-potential code does, however, encounter problems in generating computational grids in deeply recessed areas such as diverters.

Nomenclature

B	= F-16 fuselage
C_{DFRIC}	= skin-friction drag coefficient
C_{Do}	= zero-lift drag coefficient
C_{DWAVE}	= wave drag coefficient
ΔC_{DWAVE}	= incremental wave drag coefficient
D	= F-16 diverter
D_m	= modified F-16 diverter
H	= F-16 horizontal tail
STA	= longitudinal fuselage station
T	= F-16 vertical tail
W	= F-16 wing
X,Y,Z	= Cartesian coordinates

Introduction

THE development of a new fighter aircraft configuration requires detailed assessments of the zero-lift wave drag characteristics for the supersonic portion of the flight envelope. Far-field methods[1,2] have been widely used for this purpose for many years. The application of these techniques is relatively straightforward, and the required computer resources are modest. These far-field methods are most successful, however, when applied to slender configurations,[3] and problems are often encountered when analyzing nonslender fighter concepts.[4] To assess more accurately the zero-lift wave drag of such configurations, the aerodynamic designer must look to the nonlinear aerodynamic methodologies.

The nonlinear methodologies include methods based on the Navier-Stokes, Euler, and full-potential equations. Due to computer limitations, the application of the full Navier-Stokes equations to arbitrary and complex geometries is not yet practical, but significant progress has been made using the thin layer approximation.[5] Euler solvers also require substantial computer resources and are somewhat restricted in the complexity of the configurations that can be analyzed.[6] Impressive advances are being made, however, in the application of the Euler equations to practical problems in aircraft design,[7] and combinations of Euler and linear theory methods have proved useful for designing a fighter aircraft wing.[8]

Techniques based on the full-potential equation offer an attractive alternative to the Euler equations approach. The full-potential techniques are capable of providing results equivalent to the Euler results when the assumptions of irrotational and isentropic flow are valid.[9] A significant reduction in computer resources also occurs relative to the Euler solvers when the full-potential method is selected.

Two computer codes that solve the full-potential equation for supersonic flows are the NCOREL code[10] and the SIMP code.[11] NCOREL (Nonconical Relaxation) solves the nonconservative finite-difference form of the full-potential equation. Embedded and bow shocks can be predicted as well as the formation of supercritical crossflow regions. The SIMP code (Supersonic Implicit Marching Program) numerically solves the conservative form of the full-potential equation for supersonic flows with embedded regions of subsonic flow. An implicit finite-difference method based on the characteristic theory of signal propagation is employed.

NCOREL has progressed to the point where it can be applied to relatively realistic aircraft such as a fighter configuration.[12] The SIMP code has been applied to fighter configurations, the space shuttle orbiter, and the space shuttle orbiter/external fuel tank assembly.[13]

The purpose of this paper is to present and discuss the results of several zero-lift wave drag analyses conducted using the SIMP full-potential methodology.[11] The primary emphasis in these studies has been to apply the full-potential methodology to complex and realistic configurations at zero-lift and to compare these results with similar analyses conducted using the far-field (area rule) methodology.[1,2] (Reference 14 presents the results of additional full-potential code analyses at lifting conditions.)

Discussion

The design iterations for a fighter configuration require numerous wave drag assessments for drag buildup and performance analyses. The methodology selected for these assessments must be accurate, applicable to complex geometries, and not require an unusually high level of user expertise to achieve timely and accurate results. Of equal importance is the requirement that the modeling process allow convenient and rapid geometry modifications as the configuration is refined.

Received Oct. 9, 1986; presented as Paper 86-2627 at the AIAA Aircraft Systems, Design and Technology Meeting, Dayton, OH, Oct. 20–22, 1986; revision received Feb. 25, 1987.

*Program Manager, Analytical Aeronautics, Technology Division. Senior Member AIAA.

†Engineer, Technology Division. Member AIAA.

The two methodologies chosen for the present analyses meet the given requirements. The far-field area rule technique[1,2] has been widely used for both wave drag analysis and fuselage area distribution optimization. The selected full-potential code[11] is a relatively new capability that offers significant potential for improved supersonic analyses not only at zero lift but also at the higher angles of attack where aerodynamic nonlinearities may be critically important.

Methodology

The full-potential method used in the present paper has been described in detail in a number of papers[9,11,13,15,16] and thus will only be summarized here. The numerical method solves the full-potential equation in conservation form for the supersonic flow past arbitrary and complex geometries. Configurations that can be treated may include a fuselage, canopy, wing, canard, nacelle, vertical and horizontal tails, and inlets. A flux linearized upwind differencing technique is employed to advance the marching solution along the length of the configuration. The finite-difference equations are solved using an implicit factorization scheme. Embedded subsonic regions are treated using conservative switching operators to make the transition from the supersonic marching algorithm to a subsonic relaxation technique. Computational grids between the body surface and a user-specified outer boundary are developed using an elliptic grid generation routine. Boundary conditions require no net normal flow at the body surface and freestream conditions at the outer boundary, which is set outside the bow shock location. A starting data plane is established near the nose of the configuration to initiate the solution. For sharp-nosed configurations, conical starting solutions are generated, while for blunt noses a method based on the axisymmetric unsteady full-potential equation[17] is employed.

The geometry modeling requirements of this method are particularly attractive and contributed significantly to the selection of this code. Analytical descriptions of the configuration are not required. Instead, a surface description of a number of configuration cross sections is specified on a point-by-point basis. This type of geometry information is readily obtainable during the early stages of a configuration design and allows for efficient updates to the numerical model as the configuration is modified and refined. The cross section defining points are splined by the code to obtain complete cross section definitions, and linear interpolation is employed in the streamwise direction for marching plane locations between the input stations.

This full-potential method solves the entire flowfield between the body surface and the outer boundary. The program output consists of velocity components and pressure coefficients at all grid points. The overall force and moment components on the configuration are determined by integrating the computed pressure over elemental surface areas determined from the grid spacing.

The far-field methodology is based on the supersonic area rule wherein a number of equivalent bodies of revolution are generated by passing a series of cutting planes inclined at the freestream Mach angle through the configuration for a series of roll angles. The area at each station of a given equivalent body is the projection of the intercepted area onto a plane normal to the aircraft axis. The wave drag of each equivalent body is then computed using the von Kármán slender body theory. These equivalent body results are integrated over the various roll angles to obtain the total wave drag for the configuration.

The geometry modeling for the far-field methodology may be done in two ways. In the first,[1] standard components (wing, fuselage, pods, fins, tail/canard) are described in a compact manner using planform descriptions in conjunction with area and thickness distributions. In the second,[2] a completely arbitrary model may be specified using surface point descriptions.

In contrast to the full-potential approach, the far-field methodology provides only wave drag levels. No details of the aircraft flowfield or surface pressure distributions are computed. The far-field approach can be used, however, to compute the optimum (i.e., minimum wave drag) area distributions for the design of a given configuration. The opportunity thus exists to employ these techniques in a complementary manner to obtain the required performance data for a given configuration or to design and validate minimum wave drag concepts.

Supersonic Cruise Configuration Analysis

Figure 1 illustrates a supersonic cruise configuration for which a set of both pressure data and force and moment data are available.[18,19] This Mach 3.0 design employs a fuselage with highly noncircular cross sections and a modified arrow wing planform with a leading-edge sweep of 75 deg inboard and 60 deg in the wing tip region. A chine extends aft from the fuselage nose and blends into the wing leading edge at the wing side-of-body location. A minimum-drag wing twist and camber distribution is employed for improved supersonic performance. Other configuration components include flow-through nacelles located at the 31% wing semispan location, twin vertical tails mounted atop the wing where the leading-edge sweep changes from 75 to 60 deg, and a ventral fin mounted on the aircraft plane of symmetry.

The model geometry was measured on a three-axis dimension-recording machine to obtain accurate details of the model as tested. These measured geometric values were used to develop the numerical models for the analyses presented herein.

The full-potential and far-field wave drag methodologies were used to analyze the wing-body configuration of this concept at Mach numbers of 2.3, 3.0, and 3.3. The nacelles, vertical tails, and ventrals were omitted. Typical computational grids for the full-potential analysis are illustrated in Fig. 2. Grid densities ranged from 25×29 to 32×61 (normal to body x circumferential) as the solution progressed down the length of the configuration. At each cross section, the gridding was specified in two regions, with the dividing line being the normal grid line which emerges from the wing tip.

These selected grid densities were based on both previous experience with the code and in-house studies on the effect of the grid density on the overall solution. Nominal 20×30 cross section grids provide sufficient accuracy for the forward portions of most fighter-type configurations. The emergence of canards, wings, inlets, and horizontal and vertical tails requires increases in the circumferential grid density to maintain a reasonable grid distribution. The normal density is usually increased as the configuration is traversed longitudinally to maintain the grid resolution as the distance between the outer boundary and body surface increases. In

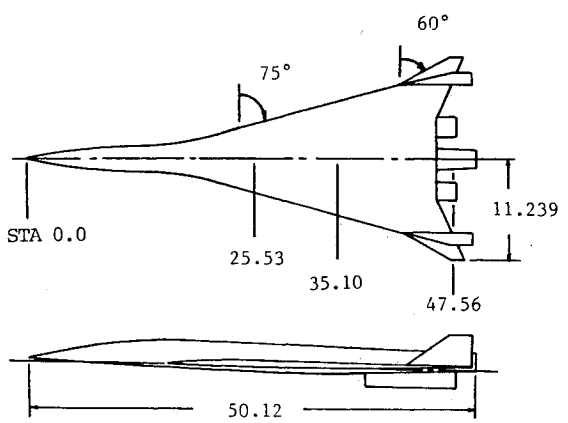

Fig. 1 Supersonic cruise configuration.

order to accurately assess the wave drag level, 700–1000 marching steps are needed.

The far-field solutions were obtained using 80 cutting planes for the development of 36 equivalent bodies of revolution (18 on each side of the vertical plane of symmetry). These values were selected based on previous experience with the far-field code as applied to fighter configurations.

Zero-lift drag estimates for this configuration were developed by combining the full-potential or far-field wave drag results with an estimate of the model skin friction computed using the T' method.[20] Zero-lift drag coefficients for the wing-body configuration are compared in Fig. 3 with test data at Mach 2.3 and 3.0. The wing-body was not tested at Mach 3.3. At Mach 2.3, the full-potential-based zero-lift drag coefficient is about two drag counts low (1 count = 0.0001), whereas the far-field method underpredicted by some seven counts. At Mach 3.0, the full-potential result is within two counts of the test value, but the far-field result is eight counts low. There is a difference of eight counts between the two methods at Mach 3.3.

These results demonstrate the applicability and accuracy of the full-potential method for zero-lift wave drag computation. In this case, the full-potential method provides a more accurate estimate of the wave drag than the far-field approach if the computed level of skin friction is accepted. The approach adopted here to form the zero-lift drag from the skin-friction and wave drag levels is applicable due to the absence of camber drag, as may be seen by examining the wind tunnel drag polars.[18]

Advanced Fighter Concept

The advanced fighter concept shown in Fig. 4 was analyzed at Mach numbers from 1.3 to 2.2. This configuration employs a relatively blunt-nosed fuselage, a cambered wing with a leading-edge sweep of 55 deg, fuselage-mounted inlets, and canted twin vertical tails. In addition, the wing sections are of the supercritical type with a large leading-edge radius.

Two modifications were made to this configuration to allow analysis using the full-potential code. The version of the code which was available for this effort could not model the side-mounted inlets with flow-through boundary conditions at the inlet face. To overcome this problem, the inlet faces were faired over to divert the flow around the inlet rather than allowing it to enter. Figure 5 illustrates this fairing. The computed wave drag must be corrected for this fairing to obtain the actual levels for performance analysis. This incremental correction can be determined from the far-field methodology or from another applicable technique.

The second geometry modification is illustrated in Fig. 6. To allow the generation of usable grids around the vertical tails, a small fillet was added as shown to relieve the severity of the corner formed by the vertical tail and the wing wake. The grid generation algorithm employed in the full-potential code works very well in most cases, but it does encounter problems in recessed regions such as this.

Typical computational grids for the full-potential analysis are shown in Fig. 7. Grid densities ranged from 30×33 to 50×47. The distance between the body surface and the outer boundary located just outside of the fuselage nose shock necessitated the use of a relatively large number of normal grid points for the adequate resolution of the flowfield. The far-field analysis employed 80 cutting planes and 36 roll angles for equivalent body determination.

The wave drag coefficients vs the Mach number for the advanced fighter are shown in Fig. 8. The inlets were faired for both the full-potential and far-field analyses.

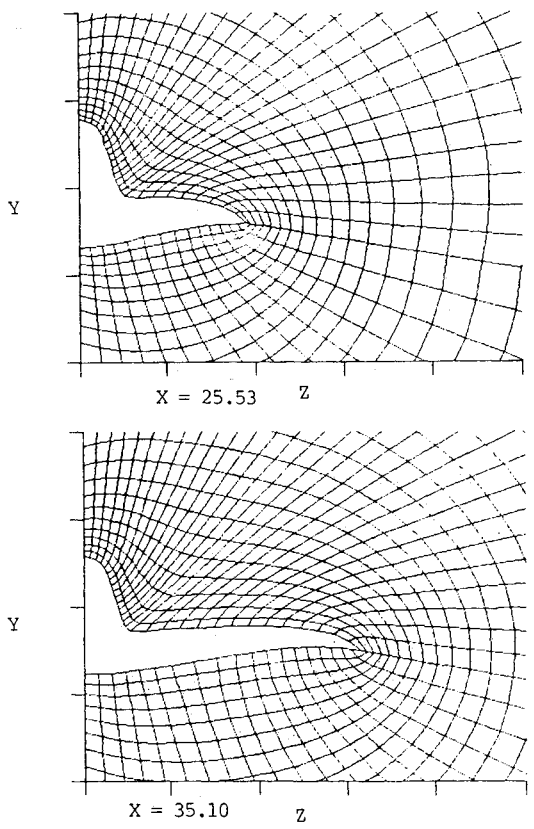

Fig. 2 Typical computational grids for the supersonic cruise wing-body configuration.

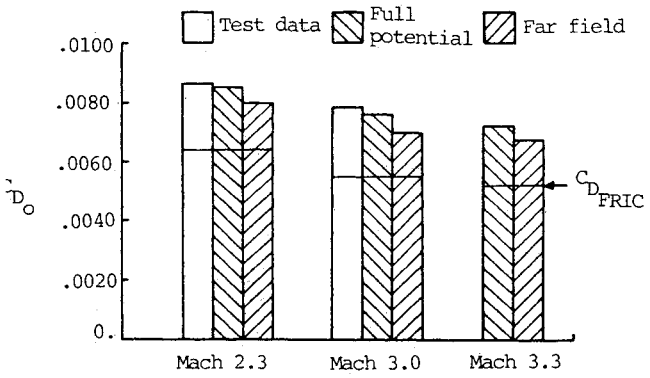

Fig. 3 Zero lift drag for the supersonic cruise wing-body configuration.

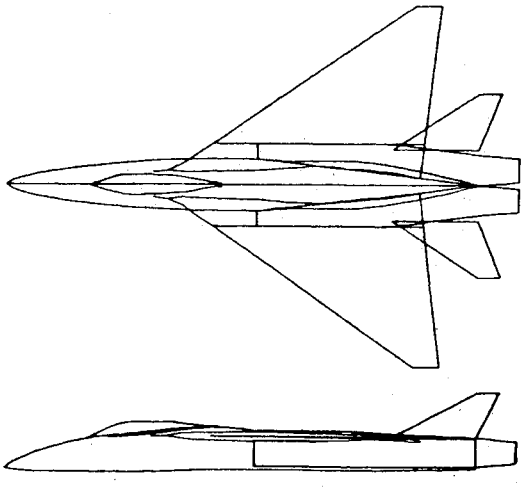

Fig. 4 Advanced fighter concept.

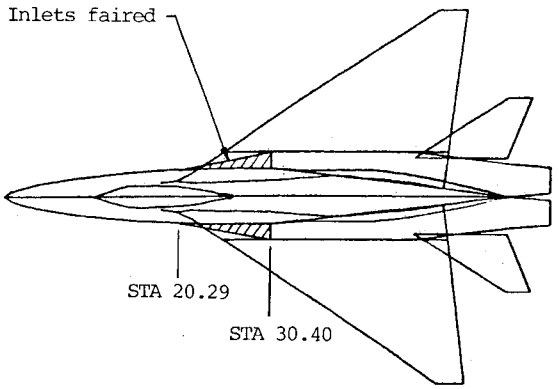

Fig. 5 Inlet fairing for full-potential code analysis.

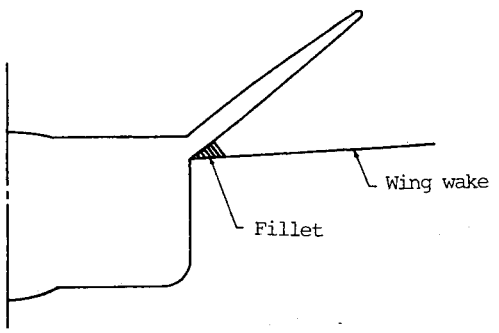

Fig. 6 V-tail fillet for full-potential code analysis.

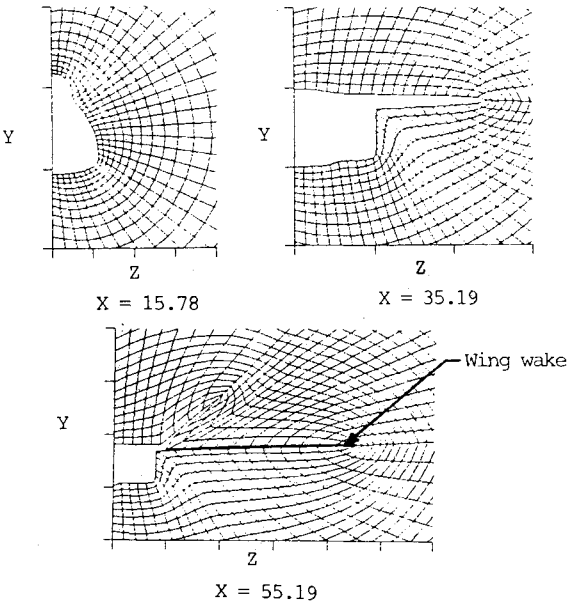

Fig. 7 Typical computational grids for the advanced fighter.

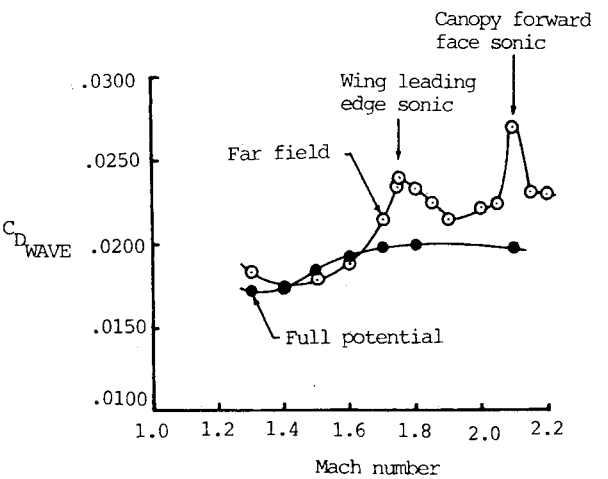

Fig. 8 Wave drag for the advanced fighter with inlets faired.

At the lower Mach numbers, the two methods agree relatively well. Above Mach 1.6, however, a significant variance in the results is observed. The far-field method encountered problems in accurately computing the wave drag at Mach 1.75, where the wing and tail leading edges are sonic, and again at Mach 2.1, where the canopy forward face is sonic. Not only are the computed drag "spikes" physically unrealistic, but the overall wave drag level in the vicinity of the sonic-condition Mach numbers appears to be adversely affected. The full-potential results vary smoothly with Mach number and do not exhibit such "spikes." In practical applications, the full-potential code could be used to develop the complete wave-drag Mach-number curve or, for a more cost-effective approach, to establish the drag level at the sonic conditions for a more reasonable fairing of the far-field results.

F-16 Analysis

The F-16 configuration is very complex geometrically and incorporates a deeply recessed diverter as well as numerous surfaces (wing, tails, and ventrals), as shown in Fig. 9. The inlet configuration was within the capability of the full-potential code, but the grid generation failed in the inlet-diverter region, as shown in Fig. 10. Numerous attempts to rectify this problem without modifying the configuration geometry were unsuccessful. In some cases grids were successfully generated, but the grid lines were highly nonorthogonal and the cells had large aspect ratios which caused the marching algorithm to fail to proceed satisfactorily. As previously discussed, the present gridding algorithm simply cannot generate usable grids for deeply recessed regions.

Figure 11 illustrates the diverter modifications made to allow the generation of usable grids. The cross section shown corresponds to the diverter leading-edge station. The modified diverter has a blunt face which was modeled as part of the inlet geometry with a flow-through boundary condition. This geometry modification extends aft about 10% of the overall fuselage length to a point where the lateral extent of the diverter allows successful grid generation. As previously discussed for the advanced fighter, an incremental correction for this geometry modification must be determined to establish the absolute wave drag level.

The complexity of the rear portion of the F-16 presented additional problems. The combination of fuselage, wing wake, horizontal tail and wake, vertical tail and wake, and the ventrals and their wakes resulted in modeling problems that could not be handled by the current version of the code. This version did not allow a respace/restart (i.e., the changing of the grid arrangement and restarting of the marching solution) when wakes were present. Thus it was necessary to define a single grid arrangement and force it to accommodate the various components and their wakes. In order to proceed with the F-16 analysis, the ventrals and vertical tail were removed to reduce the geometric complexity, and solutions were obtained for the wing-fuselage-horizontal tail configuration.

Typical computational grids are illustrated in Fig. 12. These grids ranged from 20×29 forward to 28×43 on the rear portion of the aircraft. As shown in Fig. 12c, the wing wake is forced to align with the horizontal tail for modeling and computational purposes.

Figure 13 summarizes the wave drag results for the F-16. The full-potential and far-field values (80 cutting planes, 36 roll angles) for the wing-fuselage-horizontal tail with the modified diverter are indicated by the filled circles and the solid line, respectively. These two results differ by some 60 drag counts over the Mach number range investigated. This discrepancy again points to the difficulties that can be encountered when applying the far-field methodology to nonslender fighter concepts.

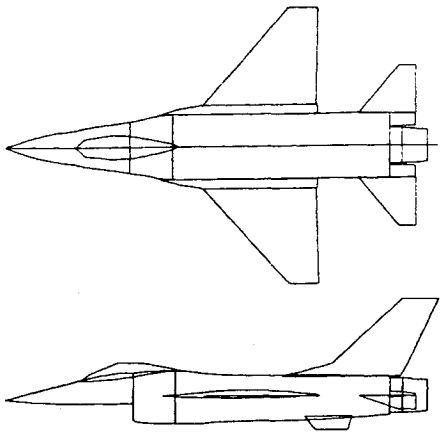

Fig. 9 F-16 configuration geometry.

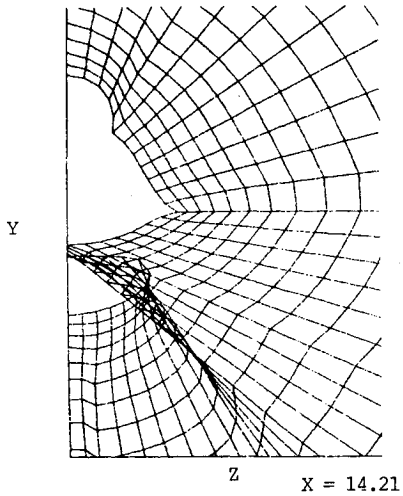

Fig. 10 Grid generation failure for the diverter/inlet geometry.

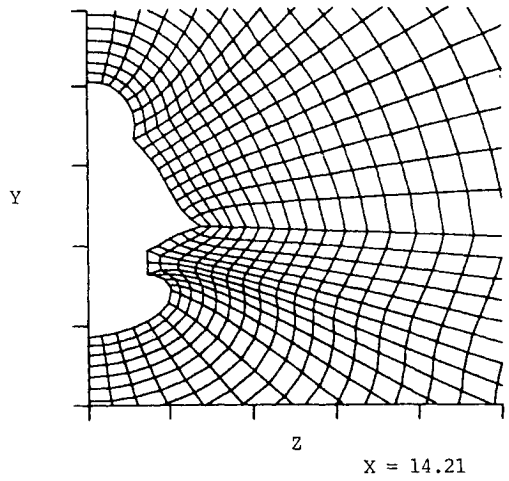

Fig. 11 Diverter modification for the full-potential code analysis.

Insight into the relative accuracy of the full-potential and far-field results for the F-16 may be obtained from Figs. 13 and 14. Shown in Fig. 13 is the far-field result for the actual F-16 configuration (ventrals off). The difference between the two far-field curves represents the wave drag increment due to the vertical tail and the diverter modification. Adding this increment to the full-potential result gives an adjusted level of wave drag for the actual configuration based on the full-potential methodology. Although the far-field method gives a low absolute wave drag level, this method can be used for estimating the incremental change associated with a given configuration variation. Alternatively, another approach could be employed, e.g., a near-field method.[21] The application of the full-potential method to the actual geometry is the desired approach, of course, so that these incremental corrections are avoided completely.

The full-potential and far-field wave drag results were combined with an estimate of the configuration skin friction[20] and are compared with measured zero-lift drag coeffi-

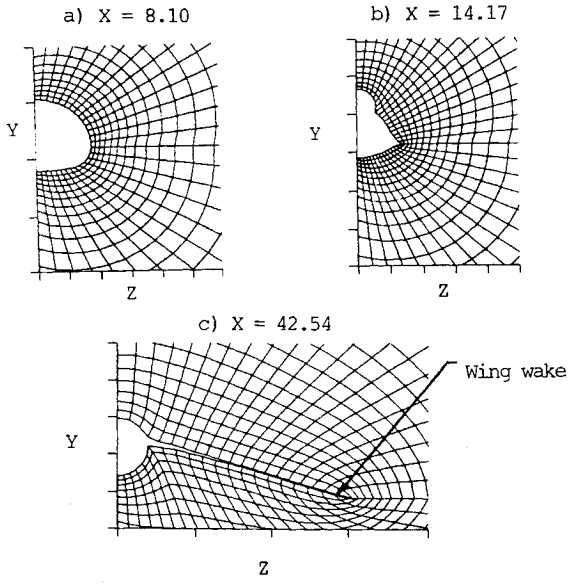

Fig. 12 Typical computational grids for the F-16.

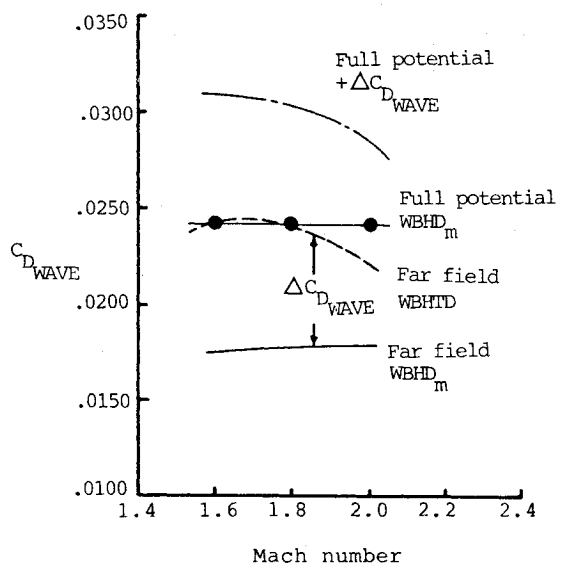

Fig. 13 F-16 wave drag summary.

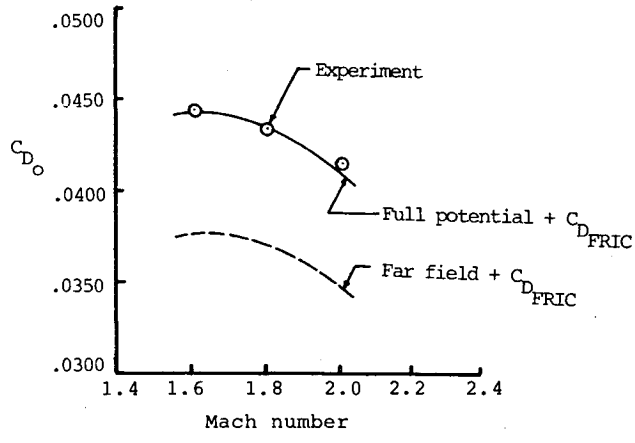

Fig. 14 F-16 zero-lift drag.

cient data[22] in Fig. 14. The experimental data are for the F-16 without the ventral fins and have been corrected to remove the zero-lift drag increment due to the wing tip missiles and launchers.[23] As Fig. 14 shows, the wave drag level based on the full-potential results agrees very well with the measured values whereas the far-field result is much lower. If the computed skin-friction and incremental wave correction levels are accepted, it may be concluded that the full-potential methodology has provided more accurate estimates of the supersonic wave drag.

Concluding Remarks

Wave drag coefficients for several aircraft configurations have been computed using a full-potential method and have been compared with the results of parallel far-field analyses and experimental zero-lift drag data. The aircraft analyzed included a supersonic cruise wing-body configuration, an advanced fighter concept, and the F-16.

The results of these studies generally indicated that the full-potential method computed more accurate wave drag levels than did the far-field technique. The full-potential method did not encounter difficulties when sonic conditions occurred on the wing or tail leading edges or on the canopy forward face, as did the far-field method.

Acknowledgment

This work was supported by the Directorate of Design Analysis, Deputy for Development Planning, Aeronautical Systems Division, Air Force Systems Command, Wright-Patterson Air Force Base, Ohio, under Contract F33615-83-0130, Task 0130-26.

References

[1]Harris, R.V. Jr., "An Analysis and Correlation of Aircraft Wave Drag," NASA TM X-947, 1964.

[2]Craidon, C.B., "User's Guide for a Computer Program for Calculating the Zero-Lift Wave Drag of Complex Aircraft Configurations," NASA TM 85670, 1983.

[3]Baals, D.D., Robins, A.W., and Harris, R.V. Jr., "Aerodynamic Design Integration of Supersonic Aircraft," AIAA Paper 68-1018, 1968.

[4]Carlson, H.W. and Harrison, R.V. Jr., "A Unified System of Supersonic Aerodynamic Analyses," NASA SP-228, "Analytic Methods in Aircraft Aerodynamics," 1969.

[5]Rizk, Y.M. and Ben-Shmuel, B., "Computation of the Viscous Flow Around the Shuttle Orbiter at Low Supersonic Speeds," AIAA Paper 85-0168, 1985.

[6]Moitra, A., "Numerical Solution of the Euler Equations for High-Speed, Blended Wing-Body Configurations," AIAA Paper 85-0123, 1985.

[7]Chakravarthy, S.R. and Szema, K.Y., "An Euler Solver for Three-Dimensional Supersonic Flows with Subsonic Pockets," AIAA Paper 85-1703, 1985.

[8]Ross, J.M., Reaser, J.S., and Bouchard, E.E., "Optimization of a Supersonic Wing by Combining Linear and Euler Methods," SAE Paper 851791, 1985.

[9]Shankar, V. and Osher, S., "An Efficient Full-Potential Implicit Method Based on Characteristics for Supersonic Flows," *AIAA Journal,* Vol. 21, Sept. 1983.

[10]Siclari, M.J., "The NCOREL Computer Program for 3D Nonlinear Supersonic Potential Flow Computations," NASA CR 3694, 1983.

[11]Shankar, V., Szema, K.Y., and Bonner, E., "Full Potential Methods for Analysis/Design of Complex Aerospace Configurations," NASA CR 3982, 1986.

[12]Siclari, M.J. and Pittman, J.L., "Application of NCOREL to Aircraft Configurations," AIAA Paper 86-1830, 1986.

[13]Szema, K.Y., Riba, W.L., Shankar, V., and Gorski, J.J., "Computation of Supersonic Flows Over Three-Dimensional Configurations," *Journal of Aircraft,* Vol. 22, Dec. 1985.

[14]Walkley, K.B. and Smith, G.E., "Application of a Full Potential Method to Practical Problems in Supersonic Aircraft Design and Analysis," Paper ICAS-86-1.4.5, *Proceedings of the 15th Congress of the International Council of the Aeronautical Sciences,* London, England, Sept. 7–12, 1986.

[15]Shankar, V., "Conservative Full Potential, Implicit Marching Scheme for Supersonic Flows," *AIAA Journal,* Vol. 20, Nov. 1982.

[16]Shankar, V., Szema, K.Y., and Osher, S., "Treatment of Supersonic Flows with Embedded Subsonic Regions," *AIAA Journal,* Vol. 23, Jan. 1985.

[17]Shankar, V., Ide, H., and Gorski, J., "Relaxation and Approximate Factorization Methods for the Unsteady Full Potential Equation," Paper ICAS-84-1.6.2, *Proceedings of the 14th Congress of the International Council of the Aeronautical Sciences,* Toulouse, France, Sept. 9–14, 1984.

[18]Shrout, B.L. and Fournier, R.H., "Aerodynamic Characteristics of a Supersonic Cruise Airplane Configuration at Mach Numbers of 2.30, 2.96, and 3.30," NASA TM 78792, 1979.

[19]Shrout, B.L., Corlett, W.A., and Collins, I.K., "Surface Pressure Data for a Supersonic Cruise Airplane Configuration at Mach Numbers of 2.30, 2.96, and 3.30," NASA TM 80061, 1979.

[20]Sommer, S.C. and Short, B.J., "Free-Flight Measurements of Turbulent-Boundary-Layer Skin Friction in the Presence of Severe Aerodynamic Heating at Mach Numbers from 2.8 to 7.0," NACA TN 3391, 1955.

[21]Middleton, W.D. and Lundry, J.L., "A System for Aerodynamic Design and Analysis of Supersonic Aircraft. Part 1—General Description and Theoretical Development," NASA CR 3351, 1980.

[22]Dollyhigh, S.M., Sangiorgio, G., and Monta, W.J., "Effects of Stores on Longitudinal Aerodynamic Characteristics of a Fighter at Supersonic Speeds," NASA TP 1175, 1978.

[23]Dollyhigh, S.M., Foss, W.E. Jr., Morris, S.J. Jr., Walkley, K.B., Swanson, E.E., and Robins, A.W., "Development and Analysis of a STOL Supersonic Cruise Fighter Concept," NASA TM 85777, 1984.